Dynamics in the U6 RNA Intramolecular Stem−Loop: A Base Flipping Conformational Change[†,‡]

Nicholas J. Reiter, Heike Blad, Frits Abildgaard, and Samuel E. Butcher*

Department of Biochemistry, University of Wisconsin-Madison, 433 Babcock Drive, Madison, Wisconsin 53706

Received June 8, 2004; Revised Manuscript Received August 27, 2004

ABSTRACT: The U6 RNA intramolecular stem−loop (ISL) structure is an essential component of the spliceosome and binds a metal ion required for pre-messenger RNA splicing. The metal binding internal loop region of the stem contains a partially protonated C67−$^+$A79 base pair (pK_a = 6.5) and an unpaired U80 nucleotide that is stacked within the helix at pH 7.0. Here, we determine that protonation occurs with an exchange lifetime of approximately 20 μs and report the solution structures of the U6 ISL at pH 5.7. The differences between pH 5.7 and 7.0 structures reveal that the pH change significantly alters the RNA conformation. At lower pH, U80 is flipped out into the major groove. Base flipping involves a purine stacking interaction of flanking nucleotides, inversion of the sugar pucker 5′ to the flipped base, and phosphodiester backbone rearrangement. Analysis of residual dipolar couplings as a function of pH indicates that base flipping is not restricted to a local conformational change. Rather, base flipping alters the alignment of the upper and lower helices. The alternative conformations of the U6 ISL reveal striking structural similarities with both the NMR and crystal structures of domain 5 of self-splicing group II introns. These structures suggest that base flipping at an essential metal binding site is a conserved feature of the splicing machinery for both the spliceosome and group II self-splicing introns.

Dynamic motions are likely to play an important role in RNA catalysis and function, as observed in the hammerhead (*1*, *2*), hairpin (*3*), and lead-dependent (*4*) ribozymes. RNA conformational transitions are essential for ribosome function and play a significant role in the recognition of proteins, RNA, and ligands (*5*−*7*). Although RNA is widely considered to be flexible, analyses of its dynamic motions in relation to structure have been limited (*1*−*4*, *8*−*13*). Studies of RNA conformational dynamics are required to understand the correlation between structure and function.

Nuclear pre-messenger RNA (pre-mRNA) splicing is catalyzed by the spliceosome, a megadalton ribonucleoprotein complex of five small nuclear RNAs (U1, U2, U4, U5, and U6) and approximately 70 proteins (*14*, *15*). Evidence suggests that spliceosomal RNAs may have a catalytic role. U6 RNA is remarkably conserved and undergoes a large conformational transition between spliceosome assembly and activation (*16*−*19*). The formation of an intramolecular stem−loop (ISL)[1] within U6 RNA is a part of this large conformation switch required prior to the first step of splicing (*18*). A sulfur substitution at the U80 pro-S_P nonbridging phosphate oxygen within the U6 ISL RNA abolishes the first step of splicing but can be rescued by thiophillic ions such as cadmium (*20*). These data indicate that metal ion binding at the U80 nucleotide of U6 is required for the first step of splicing.

A protein-free preparation of U2 and U6 RNAs can catalyze a slow reaction that is similar to the first step of splicing (*21*). The protein-free U2−U6 reaction is significantly stimulated by the presence of a conserved pseudouridine in U2, which likely plays a role in exposing the base of the branch site adenosine (*22*, *23*). Thus, although the exact catalytic components of the spliceosome active site are not known, U2 and U6 RNAs, as well as divalent metal ions, are essential in the pre-mRNA splicing reaction (*16*, *24*−*26*).

NMR studies of the U6 intramolecular stem loop (U6 ISL) have provided an initial understanding of the structure of this metal binding domain (*27*, *28*). Metal ion binding is stereoselective for the pro-S_p oxygen of U80 at neutral pH; however, stereoselectivity of metal binding is lost upon protonation of the adjacent, highly conserved C67−$^+$A79 pair, which has a pK_a of 6.5 (*27*). Protonation of the C67−$^+$A79 wobble pair stabilizes the RNA by adding a hydrogen bond, which contributes −0.7 ± 0.3 kcal/mol of folding free energy (*28*). These data suggest that the U6 ISL conformation may be altered by proton uptake.

Although U80 is essential for pre-mRNA splicing (*24*, *29*), at pH 7.0 this nucleotide is sequestered within the U6 ISL helix and does not participate in hydrogen bonding (*27*, *28*). However, the dynamic properties of U80 reported here suggest that it may indeed participate in interactions with

[†] This work was supported by an NIH grant (No. GM65166) to S.E.B. N.J.R. received predoctoral support from the University of Wisconsin Molecular Biophysics Training Grant (No. T32 GM08293).

[‡] Structure coordinates have been deposited in the Protein Data Bank as entries 1SYZ (pH 5.7) and 1SY4 (pH 7.0).

* To whom correspondence should be addressed. E-mail: butcher@nmrfam.wisc.edu. Fax: 608-262-3453. Tel: 608-263-3890.

[1] Abbreviations: DMS, dimethyl sulfate; HSQC, heteronuclear single quantum correlation spectroscopy; ISL, intramolecular stem−loop; NMR, nuclear magnetic resonance; NOESY, nuclear Overhauser effect spectroscopy; NOE, nuclear Overhauser effect; ppm, parts per million; RDC, residual dipolar coupling; RMSD, root-mean-square deviation; TOCSY, total correlation spectroscopy; TSP, 3-(trimethylsilyl)-propionic acid-d_4, sodium salt; VS, Varkud satellite.

10.1021/bi048815y CCC: $27.50
Published on Web 10/09/2004

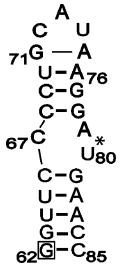

FIGURE 1: Secondary structure of the U6 ISL RNA representing nucleotides 62−85 from *Saccharomyces cerevisiae*. An asterisk (∗) denotes the location of a functionally important phosphate that binds a divalent metal ion (*20*). An A62G substitution is boxed and found to have the same overall structure as the wild-type sequence (*27*).

other components of the spliceosome, pre-mRNA, or both. NMR data indicate that an alternative U6 ISL conformation exists and is the predominating structure below pH 6.0. Structures were determined at pH 7.0 (*28*) and pH 5.7 with inclusion of residual dipolar couplings (RDCs). We find that U80 is in equilibrium between stacked and unstacked conformations and that this base movement is correlated with the protonation state of the adjacent $^{+}$A79 base. Comparisons with recent X-ray and NMR structures of a similar domain from group II introns (*30*, *31*) suggest that the observed dynamics within this metal binding internal loop region is a conserved feature of the splicing machinery for both the spliceosome and group II self-splicing introns.

MATERIALS AND METHODS

RNA Sample Preparation. The U6 ISL sequence is shown in Figure 1. RNA was prepared by in vitro transcription as previously described (*27*, *28*). Sample conditions for all NMR experiments were 0.8−1.3 mM RNA and 50 mM NaCl at pH 5.0−8.4. The pH 5.7 U6 ISL RNA sample used in the measurement of residual dipolar couplings (RDCs) was partially aligned with 7.2% C12E5/hexanol ($r = 0.96$) (*32*). C12E5 denotes an *n*-alkyl-poly(ethylene glycol) molecule, where 12 is the number of carbons in the *n*-alkyl group and 5 or 6 is the number of glycol units in the poly(ethylene glycol) moiety. Final sample conditions before and after the addition of the alignment media were 0.8−1.3 mM RNA in 300 μL (pH = 6.0). Samples were placed in thin-wall Shigemi microcell NMR tubes (Shigemi Inc.).

NMR Spectroscopy. All spectra were acquired at the National Magnetic Resonance Facility at Madison (NMRFAM) on Bruker DMX 500, 600, and 750 MHz spectrometers. CryoProbe (Bruker) single *Z*-axis gradient HCN probes were used with the 500 and 600 MHz instruments, whereas a conventional triple axis gradient HCN probe was used with the 750 MHz spectrometer. Line width and RDC measurements, as well as all NMR data for the structure determination of the U6 ISL pH 5.7, were processed using XWINNMR 2.6 software (Bruker Biospin). Resonance assignments were completed using Felix 98 (MSI) and Sparky (http://www.cgl.ucsf.edu/home/sparky). All structures were viewed and analyzed using MOLMOL (*33*).

Exchangeable proton resonances were assigned as previously described (*27*, *28*) and also by reference to 2D NOESY spectra (150 ms mixing time) in 90% H_2O/10% D_2O at 12 °C. Nonexchangeable proton resonances were assigned by reference to 2D NOESY spectra (150, 200, and 250 ms mixing times), 2D ^{1}H−^{1}H TOCSY (40 ms mixing time), and ^{1}H−^{13}C HSQC experiments collected in 99.99% D_2O at 30 °C (*27*, *28*). Despite significant chemical shift changes between pH 7.0 and 5.7, NOEs were unambiguously assigned using nucleotide-type specifically labeled samples and by 2D NMR spectra acquired at narrow incremental titrations of pH (5.06, 5.33, 6.21, 6.58, 6.95, 7.45, 8.21, and 8.44). The line widths of the H1′ resonances were measured using a 2D NOESY spectrum that was Fourier transformed without the use of a weighting function.

For the line shape analysis of the adenine C2 resonances, ^{1}H−^{13}C HSQC spectra at different pH (5.06, 5.33, 6.21, 6.58, 6.95, 7.45, 8.21, and 8.44) were recorded at 30 °C. Spectra were obtained with 2048 points with a sweep width of 4496 Hz in the t_2 dimension and 192 points with a sweep width of 4276 Hz in the t_1 dimension. The ^{13}C carrier was set to 148 ppm, and ^{13}C chemical shifts were indirectly referenced to the TSP ^{1}H signal at 0.00 ppm. The chemical shifts and line widths were determined from 1D ^{13}C vectors of the 2D ^{1}H−^{13}C HSQC spectra by Lorentzian deconvolution. Truncation artifacts were minimized by applying an exponential line broadening of 30 Hz to the FIDs prior to Fourier transformation. The reported line width at half-height of the A79 C2 signal was determined by subtracting 30 Hz from the deconvoluted line width.

Determination of Protonation Exchange at Nucleotide A79. The lifetimes for exchange between protonated and unprotonated states of the A79 N1 were determined by analysis of the line shape of the A79 C2 ^{13}C signal. In the fast-to-intermediate case of chemical or conformational exchange between two sites, A and B, the observed line width depends on the populations, the inherent line widths, and the rate of exchange between the two sites. The experimental NMR signal is given by (*10*, *34*, *35*)

$$S(\upsilon) = I_0 \frac{[P(1 + \tau_{ex}(p_A \pi w_B + p_B \pi w_A)) + QR]}{P^2 + R^2} \quad (1)$$

where I_0 is the intensity factor, p_A and p_B are the fractional populations of sites A and B, $\tau_{ex} = \tau_A\tau_B/(\tau_A + \tau_B)$, $P = \tau_{ex}[\pi^2 w_A w_B - (\pi(\upsilon_A + \upsilon_B) - 2\pi\upsilon)^2 + \pi^2(\upsilon_A - \upsilon_B)^2] + p_A\pi w_A + p_B\pi w_B$, $Q = \tau_{ex}[\pi(\upsilon_A + \upsilon_B) - 2\pi\upsilon - \pi(p_A - p_B)(\upsilon_A - \upsilon_B)]$, and $R = \pi(p_A - p_B)(\upsilon_A - \upsilon_B) - \tau_{ex}\pi(\upsilon_A - \upsilon_B)(\pi w_A - \pi w_B) + [\pi(\upsilon_A + \upsilon_B) - 2\pi\upsilon][1 + \tau_{ex}(\upsilon_A + \upsilon_B)]$. τ_{ex} is the exchange lifetime for the exchange between the protonated (A) and unprotonated (B) states, w_i and υ_i are the line width and frequency, respectively, of site i in hertz. The two-site exchange line shapes were simulated for different values of exchange times using a previously developed fitting program (*36*).

The apparent line widths of the A79 C2 signal in the fully protonated and fully deprotonated states were determined by assuming that the exchange lifetime is independent of pH (or p_A). This allowed for the line width derived from eq 1 to be simultaneously fit for all eight observed line widths and p_A. The parameters w_A, w_B, and τ_{ex} were determined while keeping the values for δ_A and δ_B fixed at their previously determined values (Table 1 and Supporting Information). The uncertainties in the exchange lifetimes were estimated by error propagation of the uncertainties in the experimental line width and the parameters δ_A, δ_B, w_A, and w_B.

Table 1: Chemical Exchange Associated with the Protonation of A79 at 30 °C as Reported by the A79 C2 ^{13}C Signal

pH	A79 C2 chemical shift (ppm)	A79 C2 line width at half-height (Hz)	A79 C2 fractional population,[a] p_A	exchange lifetime (μs)[b]
5.06	148.00	27.8 ± 2.0	0.972	27 ± 14
5.33	148.29	30.9 ± 2.0	0.930	16.4 ± 5.4
6.21	150.34	67.5 ± 2.0	0.639	21.8 ± 1.8
6.58	151.22	67.9 ± 2.0	0.514	20.8 ± 1.4
6.95	153.33	56 ± 5	0.215	25.4 ± 4.2
7.45	154.18	43 ± 10	0.095	36 ± 15
8.21	154.63	21 ± 4	0.030	29 ± 22
8.44	154.72	16 ± 4	0.018	22 ± 25

[a] The fractional population of site A is calculated as $p_A = (\delta_B - \delta_{obs})/(\delta_B - \delta_A)$, using $\delta_A = 147.80 \pm 0.20$ ppm and $\delta_B = 154.84 \pm 0.17$ ppm determined from a three-parameter fit of the observed chemical shift as a function of pH using $\delta_{obs} = p_A\delta_A + p_B\delta_B$, where $p_B = (1 - p_A)$ and $p_A = 1/(1 + 10^{pH-pK_a})$. The apparent p$K_a$ value obtained for protonization of A79 N1 is 6.50 ± 0.06 (Supporting Information) (*27*). [b] Lifetimes derived from fits to eq 1, using $w_A = 21.0 \pm 1.3$ Hz, $w_B = 12.5 \pm 1.3$ Hz, $\delta_A = 147.80 \pm 0.20$ ppm, and $\delta_B = 154.84 \pm 0.17$ ppm (Supporting Information).

NMR Structure Determination of the U6 ISL at pH 5.7. NMR experiments and determination of structural constraints for the solution structure of the U6 ISL at pH 5.7 were as previously described (*27*, *28*) with minor modifications. Internuclear residual dipolar couplings were measured (±2.0 Hz) at natural ^{13}C abundance in the proton (F2) and carbon (F1) dimensions of ^{1}H−^{13}C HSQC experiments. Homogeneous alignment of all samples was determined by measuring the ^{2}H splitting (~31 Hz at pH 5.7) and line width (≤2 Hz). Measured RDCs represent the difference between the ^{1}H and ^{13}C coupling for isotropic and partially aligned samples. Due to the observed dynamic nature of the U6 ISL internal loop and pentaloop (nucleotides 67, 71−75, 79, and 80) (Blad and Butcher, unpublished results), RDCs from these regions were not applied to the pH 5.7 structure calculations.

Structure Calculations. An initial set of 100 structures were calculated using CNS 1.1 (*37*) (http://cns.csb.yale.edu/v1.1), as previously described (*28*). The values of the axial (D_a) and rhombic (R) components of the alignment tensor were determined by analyzing the powder pattern distribution for each experimental RDC data set and further refined by following a grid search procedure, in which a series of structures were calculated with different rhombicities (*37*). An axial component (D_a) of −26.0 Hz and a rhombic component of 0.28 were found to be the experimentally determined values for the U6 ISL at pH 5.7.

After the initial structure calculations, the 50 lowest energy pH 7.0 and 5.7 structures were subjected to refinement in the presence of RDCs using XPLOR-NIH 2.0.6 (*38*). A weak planarity weighting function of 10 kcal·mol^{-1}·Å^{-2} was included for the Watson−Crick base pairs. The structure refinement involved cooling from 2000 to 100 K in 38 cycles of restrained molecular dynamics in Cartesian coordinate space corresponding to a total of 28 ps. During this calculation, the force constant for dipolar couplings was slowly increased from 0.001 to 0.2 kcal·mol^{-1}·Hz^{-2}. The simulated annealing was followed by 500 steps of energy minimization using the Powell algorithm in XPLOR-NIH. The lowest energy structures had no NOE (>0.5) or dihedral violations (>5°). To assess the quality of measured residual dipolar couplings, the experimental RDCs from the final converged structures were plotted against the back-calculated predicted RDC values generated from PALES (*39*). The experimental RDC errors were estimated from duplicate measurements. The experimental RDC RMSDs for the pH 7.0 and 5.7 structures (2.4 ± 0.1 and 1.7 ± 0.2 Hz, respectively) were lower than the back-calculated RDC RMSDs (2.8 ± 0.3 and 2.0 ± 0.2 Hz, respectively), indicating that the RDC data was appropriately weighted during the structure calculations (i.e., the back-calculated RDC RMSD obtained from the structures should not be more accurate than the measured RDC RMSD).

RESULTS

Exchange Lifetime Associated with Protonation of U6 Nucleotide A79. Exchange processes on the chemical shift time scale are reflected in the line width of the detected signal where the exchanging nuclei may be experiencing two or more electronic environments (*34*). The imino proton of nucleotide A79 is not directly observed due to its fast exchange with solvent. However, the C2 chemical shift is highly sensitive to protonation of the adjacent N1 atom, which has a pK_a of 6.5 (*27*).

A large chemical shift change for the A79 C2 resonance occurs between pH 5.04 and pH 8.44 (Table 1) (*27*). Additionally, the A79 C2 line width is significantly broader at intermediate pH values but remains sharp at pH values corresponding to the predominately protonated (pH 5.04) and unprotonated (pH 8.44) states. Determination of the fully protonated and deprotonated line widths of the A79 C2 signal enabled a full line shape analysis across eight pH values (Supporting Information). Other C2 atoms, such as those in nucleotides A73, A76, A82, and A81 (Figure 1), have modest chemical shift changes and are not line-broadened in this pH range (data not shown), indicating that the variation in ^{13}C line width of the C2 resonance of A79 can be directly attributed to proton exchange equilibrium.

Fitting the line width as a function of chemical shift change for the A79 C2 resonance to eq 1 reveals that exchange between the protonated and unprotonated state has a lifetime of approximately 20 μs (Table 1). Although imino proton exchange in Watson−Crick pairs occurs on the millisecond time scale (*40*), this exchange lifetime is similar to the observed exchange lifetimes for C−$^+$A pairs in other RNAs (*10*, *36*).

NMR Evidence for an Alternative Conformation below pH 6.0. Initial evidence for a dynamic internal loop in the U6 ISL was observed for the U80 nucleotide in 2D NOESY spectra acquired as a function of pH. At pH 7.0, average H1′ resonances of nucleotides in Watson−Crick base pairs have narrow line widths (6.5 ± 2.5 Hz, corresponding to a T_2 relaxation time of approximately 49 ms). In contrast, the H1′ resonance of U80 is broad (11.6 ± 1.3 Hz, $T_2 \approx 27$ ms). The H1′ line widths in Watson−Crick base pairs do not change when the pH is lowered to 6.0 (6.8 ± 3.0 Hz, $T_2 \approx 47$ ms), while the U80 H1′ resonance becomes significantly more line broadened (15.3 ± 3.4 Hz, $T_2 \approx 21$ ms).

At low pH, several new NOEs and chemical shift changes are observed within the U6 ISL internal loop. At pH 7.0, a sequential (i, $i + 1$) NOE between A79 and U80 is observed (Figure 2A). However, at pH 5.7, this sequential NOE is

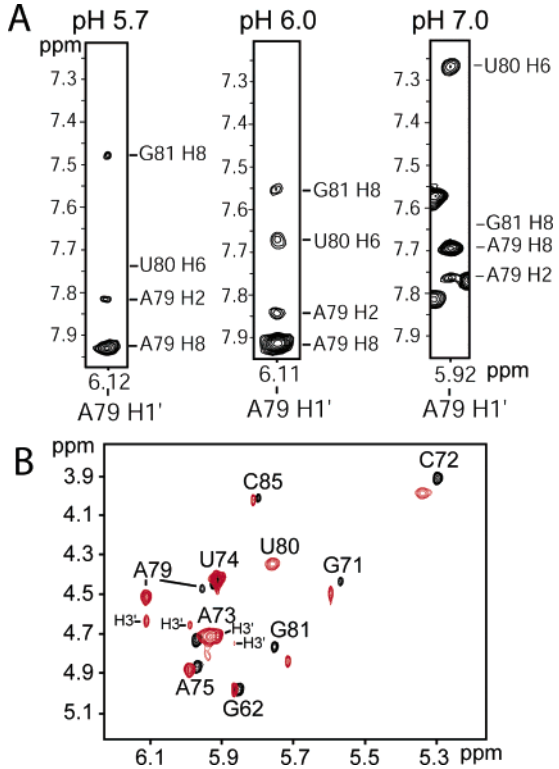

FIGURE 2: NMR evidence for a pH-induced conformational change within the U6 ISL internal loop. In panel A, the aromatic NOEs observed from the A79 H1′ resonance at pH 5.7, 6.0, and 7.0 are shown. In all strips, the chemical shifts of A79 H2, A79 H8, U80 H6, and G81 H8 are indicated. Panel B presents the 750 MHz 2D $^{1}H-^{1}H$ TOCSY spectra (40 ms mixing time) comparing H1′−H2′ and H1′−H3′ ribose proton correlations between the pH 6.0 (red) and pH 7.0 (black) U6 ISL. Unless noted, all resonances indicate an H1′−H2′ correlation.

absent, and instead, only an (i, $i + 2$) NOE between A79 and G81 is detected (Figure 2A). In addition, an aromatic stacking NOE is observed between A79 and G81 at pH 5.7 but not does occur at pH 7.0 (data not shown). At pH 6.0, both (i, $i + 1$) and (i, $i + 2$) NOEs of equal intensities are observed (Figure 2A). These data are consistent with the hypothesis that U80 is looped-out at pH 5.7 and is in conformational exchange between a stacked-in and looped-out conformation at pH 6.0. A comparison of the observed chemical shift changes as a function of pH indicate that the most pronounced changes occur throughout the internal loop, particularly at U80 (Supporting Information).

The internal loop ribose sugar puckers change as a function of pH (Figure 2B). Sugar puckers that are in the S-type range (including C2′-endo) or undergo conformational averaging give detectable H1′−H2′ scalar couplings, whereas C3′-endo sugar pucker conformations do not. At pH 7.0, the A79 pucker is conformationally averaged, as evidenced by a weak H1′−H2′ correlation (Figure 2B). In contrast, the A79 ribose displays strong H1′−H2′ and H1′−H3′ correlations at pH 6.0 and below (Figure 2B), characteristic of a C2′-endo conformation. The U80 sugar pucker is C3′-endo at pH 7.0 but undergoes conformational averaging at low pH (Figure 2B), which is consistent with increased disorder for this nucleotide at low pH.

Determination of the U6 ISL Structure at pH 5.7. The NMR data indicate that, upon a change from pH 5.7 to 7.0, a significant conformational change occurs in the U6 ISL RNA structure. To determine this conformational change, structures were calculated from the corresponding NMR data acquired at pH 5.7 and 7.0 (Table 2). At pH 5.7, the unpaired nucleotide U80 is disordered and flipped out of the helix into the major groove (Figures 3 and 4). Aside from this disorder and the previously described bulged U74 in the pentaloop (*27*), the pH 5.7 structure is well defined by NMR data (1.2 Å RMSD, Table 2).

Table 2: Statistics for the Refined U6 ISL RNA Solution Structure at 5.7 and 7.0

	pH 5.7	pH 7.0
structures:		
accepted	14	20
calculated	100	100
NOE derived distance restraints (per nucleotide)	471 (19.6)	506 (21.1)
dihedral restraints	173	180
hydrogen-bond restraints	25	25
dipolar coupling restraints	29	31
RMSD, all heavy atoms to the mean structure (Å)		
overall (62−73,75−84)	1.2 ± 0.4	0.8 ± 0.3
internal loop (66,79−80)	1.4 ± 0.5	0.4 ± 0.2
RMSD, 5 lowest energy structures (vs. pH 7.0)		
overall (62−73,75−84)	1.6 ± 0.5	
internal loop (66,79−80)	2.0 ± 0.8	
NOE violations (>0.5 Å)	0	0
avg dihedral violations (>5.0°)	0	0
avg NOE RMSD (Å)	0.037	0.027
avg dihedral RMSD (deg)	0.84	0.64
avg exptl RDC RMSD (Hz)	1.7 ± 0.2	2.4 ± 0.1
avg exptl/calcd RDC RMSD (Hz)[a]	2.0 ± 0.2	2.8 ± 0.3

[a] Determined from the lowest energy structures using PALES (*39*).

RDC measurements provide long-range distance information and are therefore excellent indicators of conformational change. Agreement between input RDC data and predicted (back-calculated) RDC values from structures is indicated by the linear correlation factor, R, and the quality factor, Q (*41*). Comparisons of the measured and back-calculated RDC values indicate that the RDC data are in agreement and consistent with the corresponding solution structures at their respective pH values (Figure 5A,D). A comparison of the measured and predicted RDC values for different pH values yields a poor correlation and a substantial increased uncertainty in the RDC data (Figure 5B,C). This poor correlation between the experimental and predicted RDC data is indicative of a global change in the orientation of $^{1}H-^{13}C$ bond vectors relative to the alignment tensor of the molecule.

DISCUSSION

Nucleotides within RNA internal loops have previously been observed to adopt stacked or looped out conformations or an equilibrium between the two (*42*−*44*). Similarly, base modifications, such as a change from a uridine to pseudouridine (ψ), can alter the base stacking conformational equilibrium of an adjacent nucleotide in RNA structure (*23*). These alternative conformations within internal loops can affect RNA tertiary folding and bending within a helix, as well as potential RNA−protein, RNA−RNA, and RNA−ligand interactions.

The comparison of U6 ISL structures at pH 7.0 and 5.7 indicates that the dynamic equilibrium within the internal

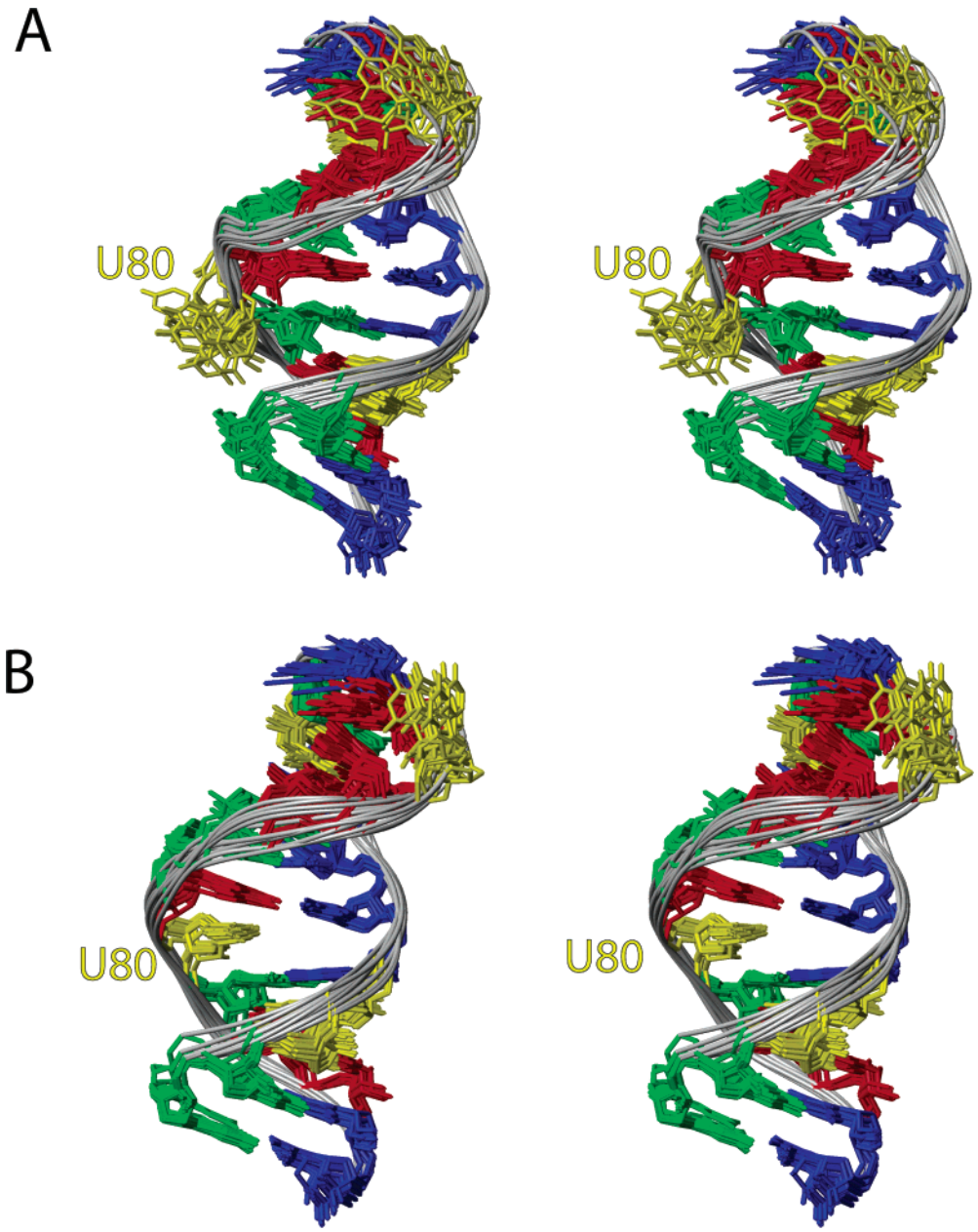

FIGURE 3: Stereoview of the NMR solution structure ensemble for the U6 ISL RNA at pH 5.7 (A) and pH 7.0 (B). Twelve pH 5.7 and pH 7.0 structures represent the lowest-energy structures from XPLOR-NIH that incorporate residual dipolar couplings (RDCs) (*38*). The phosphate backbone is designated by the gray ribbon, guanosines are green, uridines are yellow, cytidines are blue, and adenosines are red.

loop region is the likely cause of the overall global change in conformation of the RNA (Figures 3 and 4). The pH 5.7 structures reveal that U80 is displaced out into the major groove by a ~5−10 Å base movement (Figures 3 and 4). Although the largest structural change occurs within the internal loop of the U6 ISL, comparison of the structures at pH 7.0 and 5.7 reveals that base flipping produces a straight A-form helix. At pH 7.0, the unpaired U80 is intercalated into the helix and acts as a wedge to separate the $^{+}$A79−G81 stacking interaction observed at pH 5.7. The stacking of U80 into the helix is accompanied by a bend of approximately 25° (Figure 4). Helical bending is reflected in the RDC analysis, which indicates an overall change in the orientation of the ^{1}H−^{13}C bond vectors relative to the alignment tensor of the RNA (Figure 5).

Because the conformational change in the U6 ISL RNA closely correlates with the pK_a of 6.5 for the A79 nucleotide, we hypothesize that protonation of A79 influences the stacking free energy between $^{+}$A79 and G81. In vivo DMS modification data reveal that A79 is partially protected from methylation, consistent with the formation of a dynamic $^{+}$A79−C67 pair at physiological pH (*18*). Previous molecular orbital calculations of nucleic acids propose that purine−purine stacking interactions are more favorable for half-protonated pairs (i.e., one base protonated) than for nonprotonated pairs (*45*). A change in sugar pucker equilibrium within the internal loop also coincides with an alternative conformation at pH 6.0 and below. Ribose sugar puckers can flip on the nanosecond time scale for nucleotides that are free in solution or at the ends of helices (*46*, *47*). The A79 sugar pucker, which is immediately 5′ to the flipped base, favors a 2′-endo conformation at low pH (Figure 2B). Interestingly, a 2′-endo conformation 5′ to a looped out nucleotide is also observed for A73, which is positioned 5′

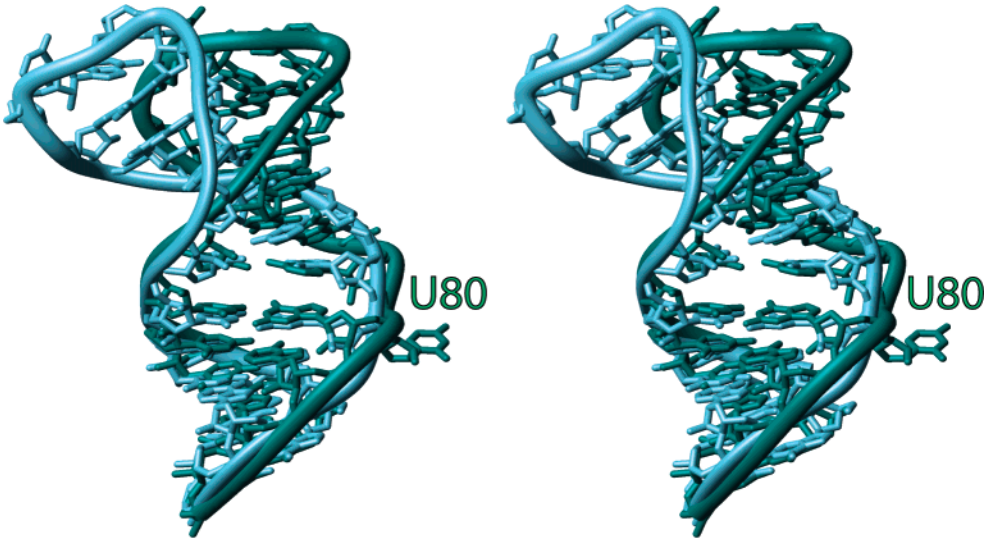

FIGURE 4: Stereo superimposition of the pH 7.0 (sky blue) and 5.7 (aqua) lowest energy U6 ISL RNA structures from the minor groove orientation. The backbone is shown as a ribbon to highlight the global change in the helical conformation. Structures superimposed over only the lower helix (nucleotides 62−66 and 81−85) have an RMSD of 0.7 ± 0.1 Å.

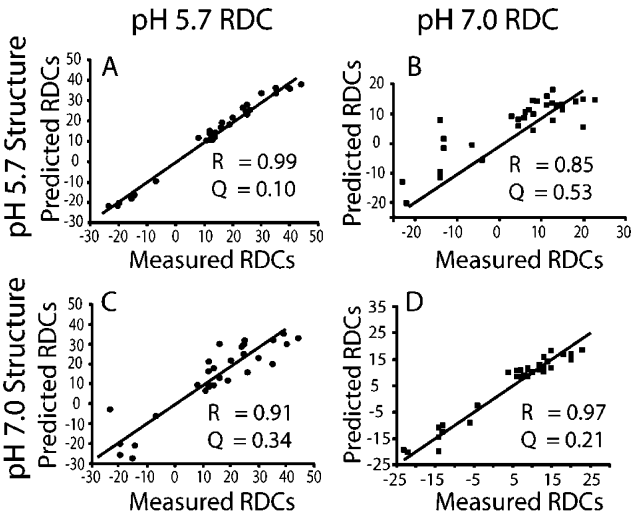

FIGURE 5: Comparison of back-calculated RDC values (vertical axis) from structures at pH 5.7 (A,B) and 7.0 (C,D) with the actual values (horizontal axis) measured at pH 5.7 (A,C) and 7.0 (B,D). The relationship between the Pearson's linearized correlation factor, *R*, and the quality factor, *Q*, is used to assess the quality of fit for each data set (*41*).

to the bulged U74 within the pentaloop (Figure 2B) (*27*, *28*). A similar relationship between bulged nucleotides and the 5′ sugar pucker has been previously observed in other RNA internal loops (*23*, *44*). Therefore, a purine−purine stacking interaction between $^{+}$A79 and G81, coupled with the 5′ sugar pucker inversion, are two structural transitions associated with base flipping of nucleotide U80. Along with these findings, NMR line shape analysis reveals that exchange dynamics between the A79 protonated and unprotonated state occur with a lifetime of approximately 20 μs (Table 1), whereas the analysis of ^{13}C $T_{1\rho}$ relaxation data show U80 structural transitions occurring on the hundred microsecond time scale (Blad and Butcher, unpublished results). Thus, A79 protonation occurs on a faster time scale than the overall conformational transition and is therefore not the rate-limiting factor that drives the base-flipping conformational change.

Effect of Protonation on the Structure and Function of RNAs. The relationship between base ionization and RNA structural flexibility is emerging as a common feature that regulates catalysis among ribozymes (*48*). For example, the Varkud satellite (VS) ribozyme contains an A−C pair (A622−C637) adjacent to the cleavage site that is thought to undergo a pH-controlled conformational switch required for substrate recognition (*49*). Additionally, the ionization state of a critical adenine (A756) within the VS ribozyme appears to play a direct role in the self-cleavage reaction mechanism (*50*). For the hepatitis δ virus (HDV) ribozyme, the ionization of an essential cytidine residue (C75) has been proposed to regulate activation of the HDV self-cleavage reaction (*51*−*54*). These studies suggest that the chemistry of some RNA catalysts is dependent upon the interplay between the local structural transitions and the ionization state of nucleobases. Other RNAs involved in gene regulatory and recognition processes may also utilize base ionization to modulate local RNA structure. The HIV-1 nucleocapsid protein (NCp7) recognition of the dimerization initiation site (DIS) RNA structure, which initiates the linkage of two homologous strands of genomic RNA during viral assembly, is coupled to adenine protonation (A272) (*55*). In this case, adenine protonation drives a conformational switch that in turn increases the rate of NCp7-catalyzed viral maturation (*55*).

Implications for Base Flipping at Nucleotide U80. Base flipping has been previously observed in DNA−protein complexes and was first reported for a cytosine-5 DNA methyltransferase binding to DNA (*56*). Molecular dynamic (MD) simulations of a DNA dodecamer containing the target sequence of DNA C5-methyltransferase suggest that base flipping is likely to favor the major groove direction and is associated with significant backbone and stacking conformational changes upon opening (*57*). Although the present study involves the dynamics of an unpaired nucleotide in RNA, there exist striking similarities with the DNA−methyltransferase complex. Both processes favor a major groove base movement, have motions on the microsecond to millisecond time scale (Blad and Butcher, unpublished

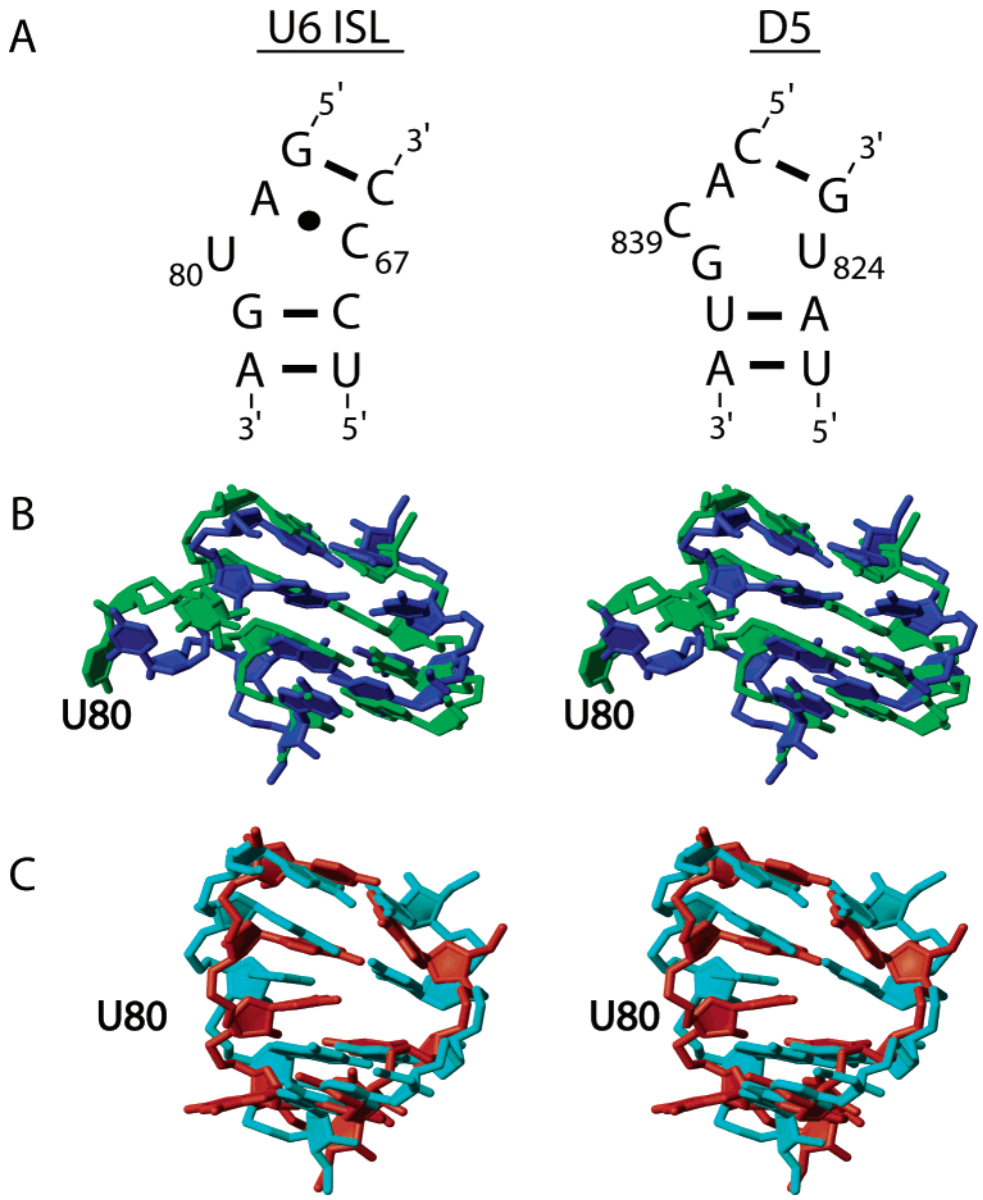

FIGURE 6: Panel A shows the secondary structure of the internal loop regions of the yeast U6 ISL RNA and domain 5 (D5) of a group II intron from yeast mitochondria (ai5γ). Panel B shows a stereo superimposition of the internal loop region (nucleotides 822−825 and 836−841) from the D5 crystal structure (green) (PDB ID 1KXK) and the lowest energy pH 5.7 U6 ISL structure (blue) (nucleotides 65−68 and 78−82). The internal loop RMSD (backbone atoms only) between the two structures is 2.8 ± 0.3 Å. Panel C shows the stereo superimposition of nucleotides 822−824 and 837−841 from the D5 NMR structure (orange) (PBD ID 1R2P) and the lowest energy pH 7.0 ISL structure (cyan) (nucleotides 65−68 and 78−82). The lowest energy pH 7.0 U6 ISL and D5 NMR structures have an RMSD of 2.7 ± 0.2 Å over internal loop backbone atoms.

results) (*57*), undergo changes in sugar pucker on the 5′ side of the opening base, and involve stacking interactions of adjacent nucleotides.

Previous mutational studies in human and yeast U6 RNA suggest that the internal loop of the U6 ISL plays a significant role in splicing. Single point mutations of U80 to G or C67 to A are lethal in yeast (*24*, *29*). The lethal U80G mutation induces formation of a C67−G80 Watson−Crick base pair, which dramatically increases the thermodynamic stability of the molecule by −3.6 ± 1.9 kcal/mol and prevents base flipping (*58*). These genetic and structural studies, along with the aforementioned metal ion binding requirement at the pro-S_P phosphoryl oxygen of U80 (*20*), emphasize the functional importance of the U6 ISL internal loop and suggest that dynamic base flipping may play an important role in splicing.

Structural Similarities with Domain 5 of Group II Introns. The spliceosome catalyzes the same splicing reactions as self-splicing group II introns. Due to functional parallels in metal binding and catalytic requirements, the highly conserved U6 ISL domain has been proposed to be analogous to domain 5 (D5) of self-splicing group II introns found in plant, fungal, and bacterial genes (*59*, *60*). D5 is also a highly conserved and essential stem−loop domain, and its internal loop region also forms a critical metal binding site (*61*). The D5 internal loop nucleotides (823−824 and 837−840) form a key minor groove tertiary contact with domain 1 and the 5′-splice site (*62*).

Despite completely different internal loop sequences (Figure 6A), we observe striking similarities between both the X-ray (*30*) and NMR (*31*) structures of D5 and the

internal loop of the U6 ISL. The crystal structure of D5 shows nucleotides A838 and C839 in flipped out conformations, similar to the flipped out U80 in the pH 5.7 U6 ISL RNA (Figure 6B). Although the internal loop region of the crystal structure is close to adjacent molecules in the lattice, the flipped out conformation of A838 and C839 is consistent with chemical probing and sequence covariation analysis (*63*, *64*). However, the NMR solution structure of D5 revealed these nucleotides to be stacked within the helix, similar to the pH 7.0 U6 ISL RNA (Figure 6C). For the D5 solution structure, it is interesting to note that exchange-broadened NOEs within the internal loop region were observed, indicative of dynamic internal motion (*31*). Comparison of the D5 NMR and crystal structures suggest that base flipping also occurs within the D5 internal loop region (Figure 6B,C). The D5 conformation does not appear to be pH-dependent as observed for the U6 ISL, perhaps due to the lack of an ionizing base within its internal loop. Nonetheless, these structures illustrate the first structural and dynamic similarities between U6 RNA and D5 of self-splicing group II introns. Interestingly, a D5 sequence is able to functionally replace the ATAC U6 ISL (*65*). Hence, the possibility exists that the U6 and D5 internal loop structures undergo related dynamic motions required for splicing.

CONCLUSIONS

Comparison of the pH 5.7 and 7.0 U6 ISL solution structures suggests that protonation of A79 favors base flipping of U80. This study provides an initial understanding of the local conformational transitions that occur within U6 spliceosomal RNA. In relation to spliceosome function, it is plausible that the looped out conformation of U80 is stabilized through formation of a tertiary interaction with (1) the U2−U6 complex, bringing the internal loop in proximity of the splice site (*20*, *66*), (2) pre-mRNA (*67*), or (3) other proteins, such as Prp8, which is a highly conserved component of the catalytic core (*68*). It will be of great interest to further expand our knowledge of the structures and dynamic processes involved in the pre-mRNA splicing mechanism.

ACKNOWLEDGMENT

The authors would like to thank Dr. Gabriel Cornilescu for discussions regarding RDC measurements and analysis, Professor Juli Feigon and Dr. Lukas Trantirek for the XPLOR-NIH refinement protocol, and NMRFAM staff for technical support. NMR studies were carried out at the National Magnetic Resonance Facility at Madison (NMRFAM) with support from the NIH Biomedical Technology Program and additional equipment funding from the University of Wisconsin, NSF Academic Infrastructure Program, NIH Shared Instrumentation Program, NSF Biological Instrumentation Program, and the U.S. Department of Agriculture.

SUPPORTING INFORMATION AVAILABLE

Supporting Information includes the A79 C2 exchange lifetime simulations, plots of the apparent line width of the ^{13}C A79 C2 signal versus the fractional population of the protonated state, p_A, and the observed change in chemical shift between pH 5.7 versus pH 7.0 U6 ISL RNA. This material is available free of charge via the Internet at http://pubs.acs.org.

REFERENCES

1. Scott, W. G., Murrary, J. B., Arnold, J. R., Stoddard, B. L., and Klug, A. (1996) Capturing the structure of a catalytic RNA intermediate: the hammerhead ribozyme, *Science 274*, 2065−2069.
2. Simorre, J. P., Legault, P., Hangar, A. B., Michiels, P., and Pardi, A. (1997) A conformational change in the catalytic core of the hammerhead ribozyme upon cleavage of an RNA substrate, *Biochemistry 36*, 518−525.
3. Zhuang, X., Kim, H., Pereira, M. J. B., Babcock, H. P., Walter, N. G., and Chu, S. (2002) Correlating structural dynamics and function in single ribozyme molecules, *Science 296*, 1473−1476.
4. Hoogstraten, C. G., Legault, P., and Pardi, A. (1998) NMR solution structure of the lead-dependent ribozyme: evidence for dynamics in RNA catalysis, *J. Mol. Biol. 284*, 337−350.
5. Valle, M., Zavialov, A., Sengupta, J., Rawat, U., Ehrenberg, M., and Frank, J. (2003) Locking and unlocking of ribosomal motions, *Cell 114*, 123−134.
6. Rodnina, M. V., Daviter, T., Gromadski, K., and Wintermeyer, W. (2002) Structural dynamics of ribosomal RNA during decoding on the ribosome, *Biochemie 9*, 849−854.
7. Noller, H., and Baucom, A. (2002) Structure of the 70S ribosome: implications for movement, *Biochem. Soc. Trans. 30*, 1159-1161.
8. Hall, K. B., and Tang, C. (1998) ^{13}C Relaxation and dynamics of the purine bases in the iron responsive element RNA hairpin, *Biochemistry 37*, 9323−9332.
9. Hoogstraten, C. G., Wank, J. R., and Pardi, A. (2000) Active site dynamics in the lead-dependent ribozyme, *Biochemistry 39*, 9951−9958.
10. Legault, P., and Pardi, A. (1997) Unusual dynamics and pK_a shift at the active site of a lead-dependent ribozyme, *J. Am. Chem. Soc. 119*, 6621−6628.
11. Dayie, K. T., Brodsky, A. S., and Williamson, J. R. (2002) Base flexibility in HIV-2 TAR RNA mapped by solution ^{15}N, ^{13}C NMR relaxation, *J. Mol. Biol. 317*, 263−278.
12. Akke, M., Fiala, R., Jiang, F., Patel, D., and Palmer, A. G., III (1997) Base dynamics in a UUCG tetraloop RNA hairpin characterized by ^{15}N spin relaxation: correlations with structure and stability, *RNA 3*, 702−709.
13. Al-Hashimi, H. M., Pitt, S. W., Majumdar, A., Xu, W., and Patel, D. J. (2003) Mg^{2+}-induced variations in the conformation and dynamics of HIV-1 TAR RNA probed using NMR residual dipolar couplings, *J. Mol. Biol. 329*, 867−873.
14. Nilsen, T. W. (1998) in *RNA Structure and Function* (Simons, R., and Grunberg-Manago, M., Eds.) pp 279−307, Cold Spring Harbor Laboratory Press, Cold Spring Harbor, NY.
15. Brow, D. A. (2002) Allosteric cascade of spliceosome activation, *Annu. Rev. Genet. 36*, 333−360.
16. Madhani, H. D., and Guthrie, C. (1992) A novel base-pairing interaction between U2 and U6 snRNAs suggests a mechanism for the catalytic activation of the spliceosome, *Cell 71*, 803−817.
17. Wolff, T., and Bindereif, A. (1993) Conformational changes of U6 RNA during the spliceosome cycle: an intramolecular helix is essential both for initiating the U4-U6 interaction and for the first step of slicing, *Genes Dev 7*, 1377−1389.
18. Fortner, D. M., Troy, R. G., and Brow, D. A. (1994) A Stem−Loop in U6 RNA defines a conformational switch required for pre-mRNA splicing, *Genes Dev. 8*, 221−233.
19. Brow, D. A., and Guthrie, C. (1988) Spliceosomal U6 RNA is remarkably conserved from yeast to mammals, *Nature 334*, 213−218.
20. Yean, S. L., Wuenschell, G., Termini, J., and Lin, R. J. (2000) Metal-ion coordination by U6 small nuclear RNA contributes to catalysis in the spliceosome, *Nature 408*, 881−884.
21. Valadkhan, S., and Manley, J. L. (2001) Splicing-related catalysis by protein-free snRNAs, *Nature 413*, 701−707.
22. Valadkhan, S., and Manley, J. L. (2003) Characterization of the catalytic activity of U2 and U6 snRNAs, *RNA 9*, 892−904.
23. Newby, M. I., and Greenbaum, N. L. (2002) Sculpting of the spliceosomal branch site recognition motif by a conserved pseudouridine, *Nat. Struct. Biol. 9*, 958−965.
24. McPheeters, D. S. (1996) Interactions of the yeast U6 RNA with the pre-mRNA branch site, *RNA 2*, 1110−1123.

25. Sontheimer, E. J., Sun, S. G., and Piccirilli, J. A. (1997) Metal ion catalysis during splicing of pre-messenger RNA, *Nature 388*, 801−805.
26. Gordon, P. M., Sontheimer, E. J., and Piccirilli, J. A. (2000) Metal ion catalysis during exon-ligation step of nuclear pre-mRNA splicing: Extending the parallels between the spliceosome and group II introns, *RNA 6*, 199−205.
27. Huppler, A., Nikstad, L. J., Allmann, A. M., Brow, D. A., and Butcher, S. E. (2002) Metal binding and base ionization in the U6 RNA intramolecular stemp-loop structure, *Nat. Struct. Biol. 9*, 431−435.
28. Reiter, N. J., Nikstad, L. J., Allmann, A. M., Johnson, R. J., and Butcher, S. E. (2003) Structure of the U6 ISL harboring a phosphorothioate modification, *RNA 9*, 533−542.
29. Madhani, H. D., Bordonne, R., and Guthrie, C. (1990) Multiple roles for U6 snRNA in the splicing pathway, *Genes Dev. 4*, 2264−2277.
30. Zhang, L., and Doudna, J. A. (2002) Structural insights into group II intron catalysis and branch site selection, *Science 295*, 2084−2088.
31. Sigel, R. K., Sashital, D. G., Abramovitz, D. L., Palmer, A. G., Butcher, S. E., and Pyle, A. M. (2004) Solution structure of domain 5 of a group II intron ribozyme reveals a new RNA motif, *Nat. Struct. Mol. Biol. 11*, 187−192.
32. Ruckert, M., and Otting, G. (2000) Alignment of biological macromolecules in novel nonionic liquid crystalline media for NMR experiments, *J. Am. Chem. Soc. 122*, 7793−7797.
33. Koradi, R., Billeter, M., and Wuthrich, K. (1996) MOLMOL: a program for display and analysis of macromolecular structures, *J. Mol. Graphics 14*, 51−55, 29−32.
34. Gutowsky, H. S., and Holm, C. H. (1956) Rate processes and nuclear magnetic resonance spectra II. Hindered internal rotation of amides, *J. Chem. Phys. 25*, 1228−1234.
35. Lane, A. N., and Lefevre, J. F. (1994) Nuclear magnetic resonance measurements of slow conformational dynamics in macromolecules, *Methods Enzymol. 239*, 596−619.
36. Ravindranathan, S., Butcher, S. E., and Feigon, J. (2000) Adenine protonation in domain B of the hairpin ribozyme, *Biochemistry 39*, 16026−16032.
37. Brunger, A. T., Adams, P. D., Clore, G. M., Delano, W. L., Gros, P., Grosse-Kunstleve, R. W., Jiang, J.-S., Kuszewki, J., Nilges, N., Pannu, N. S., Read, R. J., Rice, L. M., Simonson, T., and Warren, G. L. (1998) Crystallography and NMR System (CNS): A New Software System for Macromolecular Structure Determination., *Acta. Crystallogr. D54*, 905−921.
38. Schwieters, C. D., Kuszewki, J. J., Tjandra, N., and Clore, G. M. (2003) The Xplor-NIH molecular structure determination package, *J. Magn. Reson. 160*, 66−74.
39. Zweckstetter, M., and Bax, A. (2000) Prediction of sterically induced alignment in a dilute liquid crystalline phase: aid to protein structure determination by NMR, *J. Am. Chem. Soc. 122*, 3791−3792.
40. Gueron, M., and Leroy, J.-L. (1995) Studies of base pair kinetics by NMR measurement of proton exchange, *Methods Enzymol. 261*, 383−413.
41. Cornilescu, G., and Bax, A. (2000) Measurement of proton, nitrogen, and carbonyl chemical shielding anisotropies in a protein dissolved in a dilute liquid crystalline phase, *J. Am. Chem. Soc. 122*, 10143−10154.
42. Pan, B., Xiong, Y., Shi, K., and Sundaralingam, M. (2003) Crystal structure of a bulged RNA tetratplex at 1.1 Å resolution: Implications for a novel binding site in RNA tetraplex, *Structure 11*, 1423−1430.
43. McCallum, S. A., and Pardi, A. (2003) Refined solution structure of the iron-responsive element RNA using residual dipolar couplings, *J. Mol. Biol. 326*, 1037−1050.
44. Butcher, S. E., Allain, F. H. T., and Feigon, J. (1999) Solution structure of the loop B domain from the hairpin ribozyme, *Nat. Struct. Biol. 6*, 212−216.
45. Jordan, F., and Sostman, H. D. (1973) Molecular Orbital (CNDO/2 and MINDO) calculations on protonated deoxyribonucleic acid bases. The effects of base protonation on intermolecular interactions, *J. Am. Chem. Soc. 95*, 6544−6554.
46. Hruska, F. E., and Danyluk, S. S. (1968) Conformational changes of the ribose group in dinucleoside mono- and diphosphates: Temperature dependence, *J. Am. Chem. Soc. 90*, 3266−3267.
47. Sorin, E. J., Engelhardt, M. A., Herschlag, D., and Pande, V. S. (2002) RNA simulations: probing hairpin unfolding and the dynamics of a GNRA tetraloop, *J. Mol. Biol. 317*, 493−506.
48. Butcher, S. E. (2001) Structure and function of the small ribozymes, *Curr. Opin. Struct. Biol. 11*, 315−320.
49. Flinders, J., and Dieckmann, T. (2001) A pH-controlled conformational switch in the cleavage site of the VS ribozyme substrate RNA, *J. Mol. Biol. 308*, 665−679.
50. Jones, F. D., and Strobel, S. A. (2003) Ionization of a critical adenosine residue in the Neurospora Varkud Satellite ribozyme active site, *Biochemistry 42*, 4265−4276.
51. Ke, A., Zhou, K., Ding, F., Cate, J. H., and Doudna, J. A. (2004) A conformational switch controls hepatitis delta virus ribozyme catalysis, *Nature 429*, 201−205.
52. Perrotta, A. T., Shih, I., and Been, M. D. (1999) Imidazole rescue of a cytosine mutation in a self-cleaving ribozyme, *Science 286*, 123−126.
53. Nakano, S., Chadalavada, D. M., and Bevilacqua, P. C. (2000) General acid-base catalysis in the mechanism of a hepatitis delta virus ribozyme, *Science 287*, 1493−1497.
54. Oyelere, A. K., Kardon, J. R., and Strobel, S. A. (2002) pK_a perturbation in genomic hepatitis delta virus ribozyme catalysis evidenced by nucleotide analogue interference mapping, *Biochemistry 41*, 3667−3675.
55. Mihailescu, M. R., and Marino, J. P. (2004) A proton-coupled dynamic conformational switch in the HIV-1 dimerization initiation site kissing complex, *Proc. Natl. Acad. Sci. U.S.A. 101*, 1189−1194.
56. Roberts, R. J., and Cheng, X. D. (1998) Base Flipping, *Annu. Rev. Biochem. 67*, 181−198.
57. Varnai, P., and Lavery, R. (2002) Base flipping in DNA: Pathways and energetics studied with molecular dynamic simulations, *J. Am. Chem. Soc. 124*, 7272−7273.
58. Sashital, D., Allmann, A. M., Van Doren, S. R., and Butcher, S. E. (2003) Structural basis for a lethal mutation in U6 RNA, *Biochemistry 42*, 1470−1477.
59. Chanfreau, G., and Jacquier, A. (1994) Catalytic site components common to both splicing steps of a group II intron, *Science 266*, 1383−1387.
60. Yu, Y. T., Maroney, P. A., Darzynkiwicz, E., and Nilsen, T. W. (1995) U6 snRNA function in nuclear pre-mRNA splicing: a phosphorothioate interference analysis of the U6 phosphate backbone, *RNA 1*, 46−54.
61. Sigel, R. K., Vaidya, A., and Pyle, A. M. (2000) Metal ion binding sites in a group II intron core, *Nat. Struct. Biol. 7*, 1111−1116.
62. Boudvillain, M., de Lencastre, A., and Pyle, A. M. (2000) A tertiary interaction that links active-site domains to the 5' splice site of a group II intron, *Nature 406*, 315−318.
63. Costa, M., Christian, E. L., and Michel, F. (1998) Differential chemical probing of a group II self-splicing intron identifies bases involved in tertiary interactions and supports an alternative secondary structure model of domain V, *RNA 4*, 1055−1068.
64. Konforti, B. B., Abramovitz, D. L., Duarte, C. M., Karpeisky, A., Beigelman, L., and Pyle, A. M. (1998) Ribozyme catalysis from the major groove of group II intron domain 5, *Mol. Cell 1*, 433−441.
65. Shukla, G. C., and Padgett, R. A. (2002) A catalytically active group II intron domain 5 can function in the U12-dependent spliceosome, *Mol Cell 9*, 1145−1150.
66. Valadkhan, S., and Manley, J. L. (2002) Intrinsic metal binding by a spliceosomal RNA, *Nat. Struct. Biol. 9*, 498−499.
67. Ryan, D. E., Kim, C. H., Murray, J. B., Adams, C. J., Stockley, P. G., and Abelson, J. (2004) New tertiary constraints between the RNA components of active yeast spliceosomes: a photocrosslinking study, *RNA 10*, 1251−1265.
68. Collins, C. A., and Guthrie, C. (2000) The question remains: Is the spliceosome a ribozyme? *Nat. Struct. Biol. 7*, 850−854.

BI048815Y